Atmos. Chem. Phys., 14, 7397–7408, 2014
www.atmos-chem-phys.net/14/7397/2014/
doi:10.5194/acp-14-7397-2014

Atmospheric Chemistry and Physics
Open Access

Uptake of HO_2 radicals onto Arizona test dust particles using an aerosol flow tube

P. S. J. Matthews[1], M. T. Baeza-Romero[2], L. K. Whalley[1,3], and D. E. Heard[1,3]

[1]School of Chemistry, University of Leeds, Woodhouse Lane, Leeds, LS2 9JT, UK
[2]Escuela de Ingeniería Industrial de Toledo, Universidad de Castilla la Mancha, Avenida Carlos III s/n Real Fábrica de Armas, Toledo, 45071, Spain
[3]National Centre for Atmospheric Chemistry, University of Leeds, Woodhouse Lane, Leeds, LS2 9JT, UK

Correspondence to: D. E. Heard (d.e.heard@leeds.ac.uk)

Received: 30 January 2014 – Published in Atmos. Chem. Phys. Discuss.: 17 February 2014
Revised: 26 May 2014 – Accepted: 2 June 2014 – Published: 18 July 2014

Abstract. Uptake coefficients for HO_2 radicals onto Arizona test dust (ATD) aerosols were measured at room temperature and atmospheric pressure using an aerosol flow tube and the sensitive fluorescence assay by gas expansion (FAGE) technique, enabling HO_2 concentrations in the range $3–10 \times 10^8$ molecule cm^{-3} to be investigated. The uptake coefficients were measured as 0.031 ± 0.008 and 0.018 ± 0.006 for the lower and higher HO_2 concentrations, respectively, over a range of relative humidities (5–76 %). A time dependence for the HO_2 uptake onto the ATD aerosols was observed, with larger uptake coefficients observed at shorter reaction times. The combination of time and HO_2 concentration dependencies suggest either the partial saturation of the dust surface or that a chemical component of the dust is partially consumed whilst the aerosols are exposed to HO_2. A constrained box model is used to show that HO_2 uptake to dust surfaces may be an important loss pathway of HO_2 in the atmosphere.

1 Introduction

OH and HO_2 radicals, collectively known as HO_x, are closely coupled and together are responsible for the majority of the oxidation in the troposphere. The OH radical controls the concentrations of many species in the atmosphere such as volatile organic compounds (VOCs), whilst the HO_2 radical can react with species such as NO, O_3 and halogen oxides to recycle OH radicals. Therefore, it is important to understand the processes and reactions that control the concentrations of HO_x radicals. In a significant number of field studies a lower concentration of HO_2 has been measured than predicted using constrained box models (Brune et al., 1999; Cantrell et al., 1996; Carslaw et al., 1999, 2002; Haggerstone et al., 2005; Jaegle et al., 2000; Kanaya et al., 2000, 2007; Mao et al., 2010; Smith et al., 2006; Sommariva et al., 2004, 2006; Stevens et al., 1994; Stone et al., 2012; Whalley et al., 2010). The discrepancy between measured and predicted HO_2 concentrations has, in some cases, been attributed to heterogeneous uptake by aerosols, although some of the historical differences in the marine boundary layer (MBL) have now be accounted for by inclusion of the reactions of HO_2 with halogen oxides (Bloss et al., 2005; Kanaya et al., 2002; Sommariva et al., 2006).

Mineral dust is one of the most abundant aerosols in the atmosphere (Textor et al., 2006). Estimates suggest that 2000 Tg $year^{-1}$ are emitted into the troposphere and that it has an average residence time of 4 days before being removed by deposition (Textor et al., 2006). Mineral dust aerosols are formed from wind erosion over soil and deserts and are therefore composed of oxides and carbonates, which are found in Earth's crust. Although the main sources of mineral dust particles in the atmosphere are the North African and Asian deserts, it can be carried over thousands of kilometres by wind (Textor et al., 2006). As well as being a major source of particulate matter in the troposphere, mineral dust plays an important role in processes controlling air quality, visibility, radiative forcing, biogeochemical cycles and atmospheric chemistry (Dentener et al., 1996; Seinfeld and Pandis, 2006). The heterogeneous uptake onto dust can influence

the concentrations of several important species, for example NO_x, O_3 and HO_x (Dentener et al., 1996; Tang et al., 2014).

Arizona test dust (ATD) is a proxy for atmospheric mineral dust as it contains many of the same metals which are found in naturally occurring mineral dust aerosols, for example Saharan and Asian dust (Karagulian et al., 2006), although its mineralogy is different. The composition of ATD (Powder Technology Inc.) is SiO_2 (68–76 %), Al_2O_3 (10–15 %), Fe_2O_3 (2–5 %), Na_2O (2–4 %), CaO (2–5 %), MgO (1–2 %), TiO_2 (0.5–1.0 %) and K_2O (2–5 %). An aerosol flow tube has been used to measure the uptake coefficient for N_2O_5 upon ATD aerosols (Tang et al., 2014) but to our knowledge, only one laboratory study has measured HO_2 uptake by ATD surfaces. ATD (0–3 µm) was chosen in this work rather than Saharan dust due to the smaller size of the ATD particles which reduces the risk of aerosol deposition along the flow tube. Bedjanian et al. (2013) recently measured initial HO_2 uptake coefficients onto ATD solid surfaces for HO_2 concentrations in the range of $0.35–3.30 \times 10^{12}$ molecule cm^{-3}. However, there are currently no studies measuring HO_2 uptake coefficients onto ATD aerosols (rather than surfaces) or under atmospherically relevant HO_2 concentrations. Therefore, the aim of this study was to measure the HO_2 uptake coefficient for ATD aerosols at two different initial HO_2 concentrations (1×10^9 and 3×10^8 molecule cm^{-3}), over a range of relative humidities (6–73 % RH) and as a function of the time that the ATD aerosol particles are exposed to the HO_2 radicals.

2 Experimental

2.1 Overview of the apparatus

The experimental apparatus used to measure HO_2 uptake coefficients onto ATD aerosols at atmospheric pressure and at 291 ± 2 K is shown in Fig. 1. The majority of the apparatus is described in detail by George et al. (2013) and is therefore only described briefly here. The dust disperser produced aerosol number concentrations which were unstable over time, and were measured using a condensation particle counter (CPC; TSI 3775). Half of the experiments were performed with the CPC before the aerosol flow tube and half were performed with it after the flow tube. It was found that the position of the CPC did not affect the measured uptake coefficient indicating that losses of dust in the flow tube were negligible. The total flow through the flow tube (107 cm length, 5.9 cm I.D.) was 5.4 ± 0.2 L min^{-1} which resulted in a Reynolds number of ~ 130. Experiments were performed by placing a moveable injector (which introduced the HO_2 radicals into the flow tube) at different positions along the flow tube (30, 40, 50, 60, 70 and 80 cm) corresponding to reaction times between ~ 7 and 23 s. The distances were measured from the end of the flow tube to the injector position (a length of 0 cm would have represented the injector being at the end of the flow tube attached to the FAGE cell). For a given injector position, the HO_2 signal was then measured at the end of the flow tube using the fluorescence assay by gas expansion (FAGE) technique as a function of the aerosol concentration. The sensitivity of the FAGE cell towards HO_2 was calibrated and hence the signal could be converted into an absolute concentration (George et al., 2013).

2.2 HO_2 generation and detection

HO_2 radicals were produced by passing water vapour over a mercury lamp (L.O.T.-Oriel 6035) placed within a moveable injector (110 cm length, 1.9 cm O.D. (outer diameter), 1.6 cm I.D. (inner diameter)) via the following reactions:

$$H_2O + h\nu \rightarrow OH + H, \quad \text{(R1)}$$

$$H + O_2 + M \rightarrow HO_2 + M. \quad \text{(R2)}$$

The experiments were performed at two different initial HO_2 concentrations by setting the lamp current to either 20 or 2.5 mA, which produced initial HO_2 concentrations of 1×10^9 and 3×10^8 molecule cm^{-3} respectively, after dilution of the injector flow with the aerosol flow. A correction was applied to take into account any changes in the LIF (laser-induced fluorescence) signal owing to fluorescence quenching by water vapour if it was changed during experiments, using the methodology described by Vaughan et al. (2012). The maximum correction was an 8 % change in the HO_2 concentration. Initial HO_2 concentrations were calculated by propagating the measured HO_2 concentrations without aerosols present back to time zero (defined as the point of injection into the main flow tube). The HO_2 concentrations were also measured at the first injector position (30 cm along the flow tube, ~ 7 s) with no aerosols being present to take into account the wall loss in the first section of the flow tube.

HO_2 radicals were detected by FAGE (detection limit $\sim 10^6$ molecule cm^{-3}) which has previously been described (George et al., 2013). Briefly, the HO_2 radicals entered the FAGE cell placed at the end of the flow tube through a 0.7 mm diameter pinhole and were converted into OH by reacting with NO (BOC, 99.5 %). The $Q_1(2)$ line of the OH ($A^2\Sigma^+ - X^2\Pi_i\, v' = 0 - v'' = 0$) transition at ~ 308 nm was utilised to excite the OH fluorescence in the FAGE cell. A Nd : YAG (neodymium-doped yttrium aluminium garnet)-pumped dye laser produced the required 308 nm radiation (line width ~ 0.1 cm^{-1}) and was operated at a pulse repetition rate of 5 kHz, with a pulse energy of ≈ 2.4 µJ. The FAGE cell was continuously evacuated using a combination of a rotary pump (Edwards, model E1M80) and a roots blower (EH1200) and was kept at 0.8–0.9 Torr, which was monitored using a capacitance monitor (Tylan General, CDC 11). Mie scattering has previously been found not to contribute towards the FAGE cell signal and aerosols were found not to

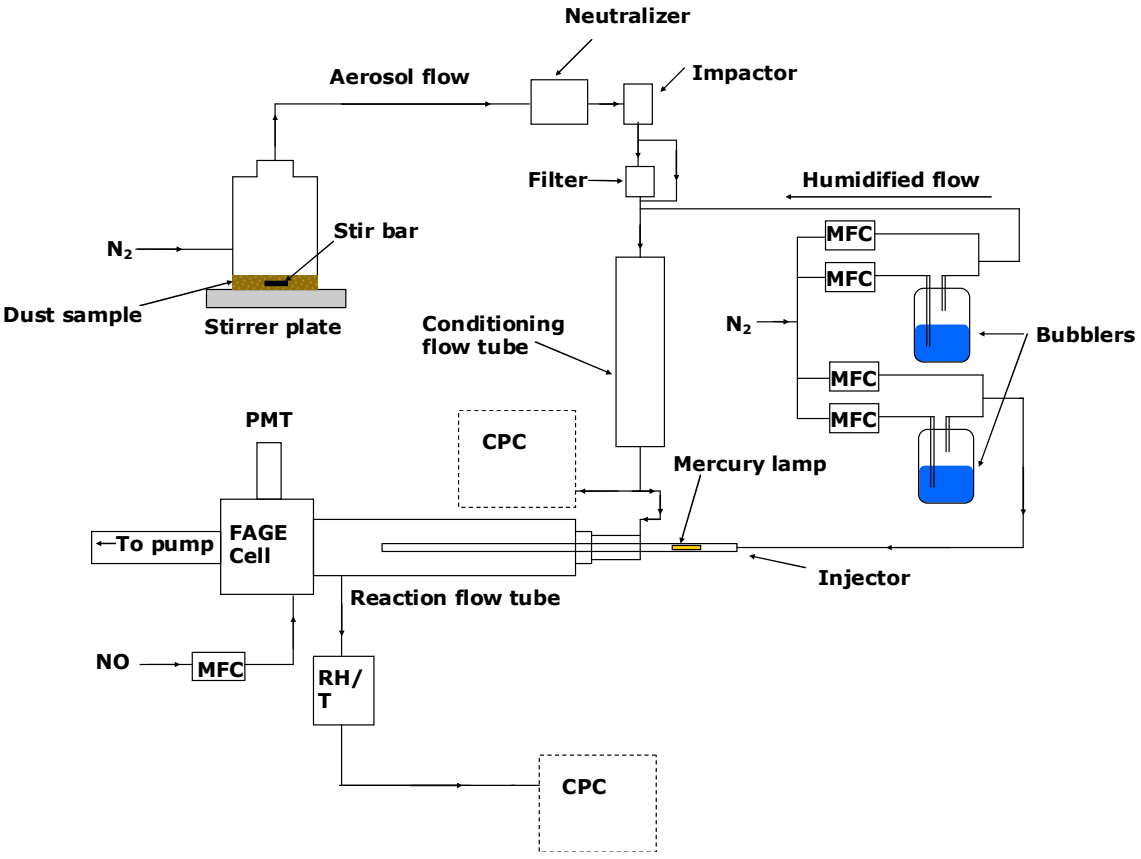

Figure 1. Schematic of the experimental setup showing the dust aerosol generator, conditioning system, aerosol flow tube and HO_2 detection system. Key: MFC – mass flow controller; CPC – condensation particle counter; PMT – photomultiplier tube; RH/T – relative humidity and temperature probe; FAGE – fluorescence assay by gas expansion. Dotted lines represent the two possible positions in which the CPC was placed. When measurements were made with the aerodynamic particle sizer and scanning mobility particle sizer, these were placed in the CPC positions.

influence the LIF detection sensitivity towards HO_2 (George et al., 2013).

2.3 Arizona test dust generation and detection

The carrier gas used for these experiments was compressed nitrogen which first passed through a gas purification system (TSI 3074B) consisting of particle filters, a dryer and a carbon filter. The HO_2 flow, the humidified flow and the NO flow were controlled using five mass flow controllers (Brooks, model 5850S and MKS, model 1179A). The required relative humidity was obtained by mixing together and altering the ratio of a dry flow and a flow which had been passed through a water bubbler. This humidified flow, which was mixed with the aerosol flow in the conditioning flow tube, varied from 3.6 L min^{-1} to 4.3 L min^{-1} but was constant throughout each individual experiment. The aerosol flow was monitored and maintained at 1.35 ± 0.05 L min^{-1} and the HO_2 flow was measured as 1.29 ± 0.02 L min^{-1}. The total flow passing through the flow tube, including the aerosol, dilution and HO_2 flows, was between 5.2 and 5.6 L min^{-1}. The FAGE instrument sampled 4.3 L min^{-1} and the CPC sampled 0.3 L min^{-1} with the remainder of the flow (0.6–1.0 L min^{-1}) exiting via an exhaust line.

The dust disperser consisted of a 500 mL high density polyethylene (HDPE) bottle (Thermo Scientific Nalgene) that had two holes drilled into it (one through the lid and one 5 cm from the base of the bottle, see Fig. 1). Two 1/4 in. O.D. tubes were placed through the holes and affixed to the bottle. Nitrogen entered the dust disperser through the tube on the side of the bottle and left through the tube at the top of the bottle. A magnetic stir bar (PTFE covered, 45 mm in length) was placed in the bottle and the bottle was placed on top of a magnetic stirrer, (Gallenkamp, 8640677) which was set to the maximum stirring speed. The combination of the stirring and the nitrogen flow produced a "dust cloud" in the bottle, which produced a non-stable aerosol concentration.

The flow of ATD aerosols passed through an impactor, which was used to stabilise the flow rate from the dust disperser. The concentration of aerosols entering the flow tube was controlled using a high efficiency particulate air

(HEPA) filter and a bypass. The proportion of the flow passing through the bypass compared to the filter was controlled using a needle valve.

The aerosol number concentration was monitored using a CPC (TSI 3775). Measurements were also made under the same experimental conditions using a scanning mobility particle sizer (SMPS; TSI, 3080) and an aerodynamic particle sizer (APS; TSI, 3321) in order to measure the entire log-normal size distribution, as shown in Fig. 2. The APS measures the time of flight of particles over a fixed distance. Therefore, corrections were made to convert the aerodynamic diameters (D_a) measured by the APS into a Stokes diameter (D_S) (measured by the SMPS) by taking into account the density of the dust particles (ρ) and the non-sphericity of the aerosols (β) (Hinds, 1982).

$$D_S = \frac{D_a}{\sqrt{\rho\beta}} \quad (1)$$

A value of $\rho = 2.7\,\mathrm{g\,cm^{-3}}$ was used for the density of Arizona test dust, and $\beta = 1.8$ produced the best agreement between the SMPS and APS size distribution, and is close to the value for Saharan dust reported by Tang et al. (2012). From Fig. 2, the average radius of a single aerosol was calculated as 273 ± 10 nm. Checks determined that the average radius did not change over time or when sampling from before or after the flow tube.

2.4 Data analysis

A clear anti-correlation between the HO_2 signal and the aerosol number concentration was observed, as shown in Fig. 3, showing that there is an interaction between HO_2 and the aerosols. When the CPC was placed before the flow tube (for half of the experiments) a dilution factor had to be applied to the aerosol number concentration to take into account the flow from the injector mixing in to the rest of the flow.

$$N_{\mathrm{flowtube}} = \frac{N_{\mathrm{CPC}}(F_{\mathrm{total}} - F_{\mathrm{HO_2}})}{F_{\mathrm{total}}}, \quad (2)$$

where N_{flowtube} is the aerosol number concentration in the flow tube, N_{CPC} is the number concentration measured by the CPC, F_{total} is the total flow entering the flow tube and $F_{\mathrm{HO_2}}$ is the total flow from the injector.

For each injector position along the flow tube, corresponding to a given value of the reaction time t, the HO_2 concentration is given by Wagner et al. (2008):

$$-\ln\frac{[\mathrm{HO_2}]_t}{[\mathrm{HO_2}]_0} = 0.25\gamma_{\mathrm{obs}} w A_d N_d t + k_w t, \quad (3)$$

where γ_{obs} is the observed HO_2 uptake coefficient, N_d is the aerosol number concentration, A_d is the average surface area of an aerosol particle assuming a spherical shape, t is the reaction time which was calculated from the flow rate, injector position and dimensions of the flow tube, k_w is the pseudo first-order wall loss and w is the mean molecular speed of HO_2 at room temperature given by

$$w = \sqrt{\frac{8RT}{\pi M_w}}, \quad (4)$$

where R is the universal gas constant, T is the temperature and M_w is the molecular weight of HO_2. Hence plotting the natural log of the HO_2 LIF signal (with any background from scattered light subtracted) against N_d, as shown in Fig. 4, yields a gradient of $-0.25\gamma_{\mathrm{obs}} w A_d t$. For each position along the flow tube, corresponding to a particular reaction time, the signal was obtained as a function of aerosol number concentration, and this included a signal with no aerosols present, and so for each reaction time the effect of wall loss was directly subtracted. Data obtained for aerosol number concentrations above 4×10^4 particles $\mathrm{cm^{-3}}$ were not included in the analysis as the FAGE signal was usually close to background levels. A graph of the gradient of Fig. 4 ($0.25\gamma_{\mathrm{obs}} w A_d t$) plotted against t yields a gradient of $0.25\gamma_{\mathrm{obs}} w A_d$, as shown in Fig. 5, from which an observed uptake coefficient could be calculated. A_d was calculated from the average radius (r_s) of the aerosols:

$$A_d = 4\pi r_s^2, \quad (5)$$

where

$$r_s^2 = A_{\mathrm{total}}/(4\pi N_{\mathrm{total}}), \quad (6)$$

where A_{total} is the total surface area measured in Fig. 2 and N_{total} is the total number of particles producing that surface area.

Unlike in previous experiments (George et al., 2013), the whole SMPS size distribution was not used to calculate the surface area, as the SMPS took 3 min to scan a distribution during which the dust aerosol number concentration varied significantly. The SMPS distribution shown in Fig. 2 is an average of many SMPS distributions, from which the average radius was obtained, and the CPC aerosol number density which was recorded with 1 s averaging period was used to calculate the average surface area with the same time distribution.

The observed uptake coefficient was corrected to take into account the effects of gas phase diffusion:

$$\gamma_{\mathrm{corr}} = \frac{\gamma_{\mathrm{obs}}}{1 - \gamma_{\mathrm{obs}}\lambda(r_s)}, \quad (7)$$

where the values of $\lambda(r_s)$ are given by

$$\lambda(r_s) = \frac{0.75 + 0.283Kn}{Kn(1+Kn)}, \quad (8)$$

where Kn is the Knudsen number defined by

$$Kn = \frac{3D_g}{w r_s}, \quad (9)$$

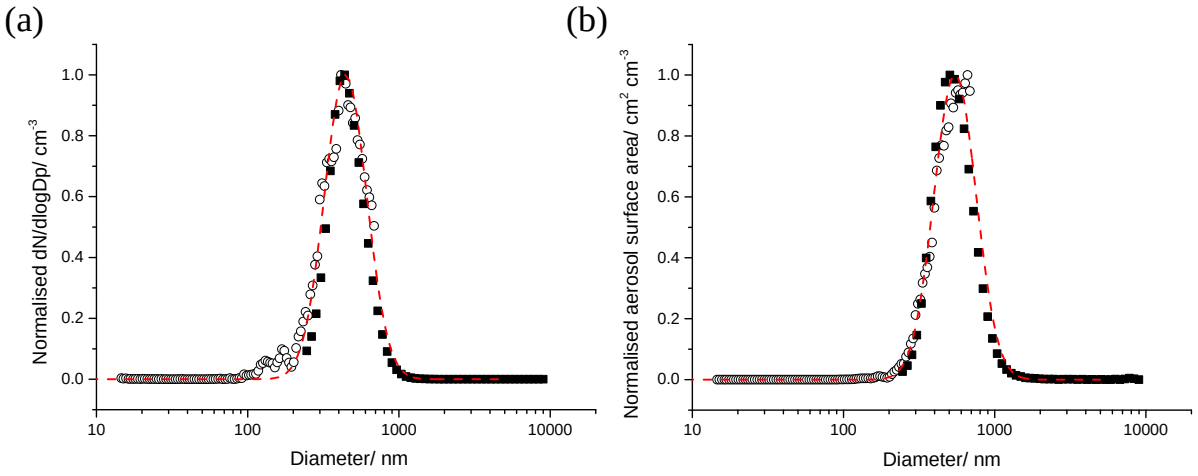

Figure 2. Normalised **(a)** number weighted and **(b)** surface weighted ATD aerosol size distributions recorded with the SMPS (open symbols) and the APS (closed symbols) positioned at the downstream end of the aerosol flow tube. The red line represents a log normal fitting to all the measured points from both instruments for the number-weighted distribution.

where D_g is the gas phase diffusion constant of HO_2 ($0.25\,cm^2\,s^{-1}$) at room temperature (Mozurkewich et al., 1987). The Brown correction (Brown, 1978) was then applied to the uptake coefficients, in order to take into account the laminar flow in the flow tube.

2.5 Measuring the time dependence of the uptake coefficient

In order to determine whether the HO_2 uptake coefficient was a function of the reaction time between HO_2 and the dust aerosol, the average uptake coefficient between the time that the HO_2 was released into the flow tube (t_0) and the time that it took to reach the FAGE cell (t) was measured. The analysis described above was used, however, instead of plotting ($0.25\gamma_{obs}wA_dt$) against t (Fig. 5), uptake coefficients were calculated for each individual injector position by using $t-t_0$ as the time in Eq. (3). This is equivalent to measuring the gradient of a line that connects the origin with each data point in Fig. 5. If the uptake coefficient was constant over time, the linear-least squares fitted line to the data shown in Fig. 5 would be expected to pass through the origin. An intercept on the y axis could indicate rapid uptake in the first few seconds of contact between the HO_2 radicals and the aerosols corresponding to a higher uptake coefficient, which then reduces over time.

3 Results and discussion

3.1 The uptake coefficient dependence on humidity and HO_2 concentration

The HO_2 uptake coefficient onto ATD aerosols was measured over the RH range 5–76 % and at two initial HO_2 concentrations of 1×10^9 and 3×10^8 molecule cm^{-3}, the data for which are shown in Fig. 6. When averaged over the range of RH studied, HO_2 uptake coefficients of $\gamma_{corr} = 0.018\pm0.006$ and 0.031 ± 0.008 were obtained for $[HO_2] = 1\times10^9$ and 3×10^8 molecule cm^{-3}, respectively. Figure 6 shows a slight increase in the uptake coefficient as the RH increases. However, it should be noted that although the HO_2 concentration exiting the injector was the same for different RH, the HO_2 signal (which was corrected for fluorescence quenching) dropped more quickly along the flow tube at higher HO_2 concentrations because of higher wall losses observed at higher RH (George et al., 2013). It was observed that by 30 cm along the flow tube, corresponding to ~ 7 s reaction time, the HO_2 concentration at 7 % RH was approximately double that of the HO_2 concentration when working at 75 % RH, for both of the initial HO_2 concentrations used. At higher RH, uptake coefficients were effectively being measured at lower HO_2 concentrations. Therefore, the apparent small increase in uptake coefficient with RH may be due to the reducing HO_2 concentration.

Uptake coefficients were then measured for different concentrations of HO_2 generated in the injector. Figure 7 shows uptake coefficients determined from gradients of Fig. 5 (HO_2 loss as a function of aerosol number concentration measured for a variety of fixed injector positions between 30 and 80 cm) plotted against the HO_2 concentration at 30 cm along the flow tube. These results show clearly that the measured uptake coefficients increase as the initial HO_2 concentration is decreased. This concentration dependence would be expected if the HO_2 radicals (or the product of a reaction of HO_2 on the dust aerosol surface, which is assumed below to be H_2O_2) were binding to the active adsorption sites (S) of the aerosols and thereby blocking further adsorption of HO_2 radicals. A potential reaction scheme is shown in

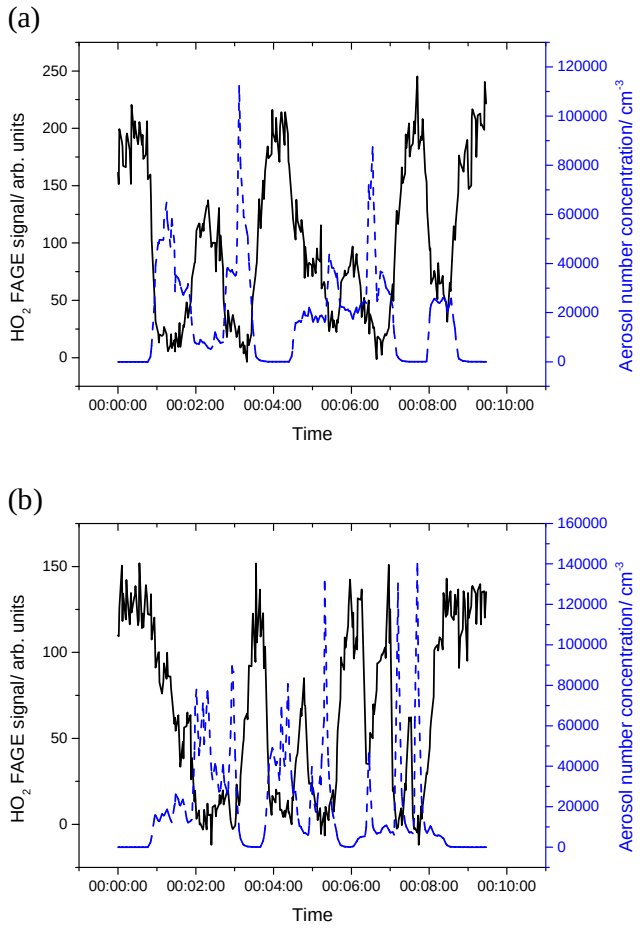

Figure 3. Two examples of the FAGE signal from HO_2 radicals (black line, left axis) together with the dust aerosol number concentration (dashed blue line, right axis), showing anti-correlations. Initial HO_2 concentrations were 1×10^9 molecule cm^{-3} for both plots but for **(a)** the injector was positioned at 70 cm and the relative humidity was 32 % whereas for **(b)** the injector was positioned at 60 cm and the relative humidity was 53 %.

Reactions (R3)–(R6):

$$HO_2(g) + S \rightleftharpoons HO_2 - S, \quad \text{(R3)}$$

$$HO_2 - S + HO_2 - S \rightarrow H_2O_2(g) + O_2 + 2S, \quad \text{(R4)}$$

$$HO_2 - S + HO_2 - S \rightarrow H_2O_2 - S + O_2 + S \quad \text{(R5)}$$

$$H_2O_2 - S \rightleftharpoons H_2O_2(g) + S. \quad \text{(R6)}$$

If the surface were becoming partially saturated with HO_2 radicals (or the products of a reaction) and blocking the incoming HO_2 radicals, a decrease in the uptake coefficient with time would then be expected. Another possible explanation for an HO_2 concentration dependence would be if the HO_2 was reacting with a trace component of the aerosol (X),

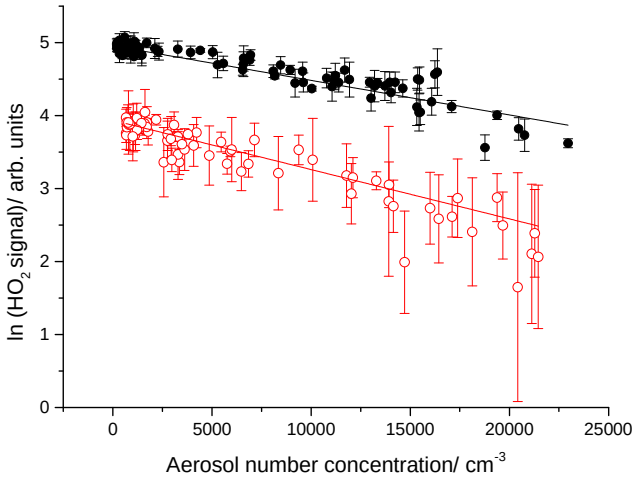

Figure 4. The exponential dependence of the measured HO_2 signal with the ATD aerosol number concentration. The data are for an initial HO_2 concentration of 1×10^9 molecule cm^{-3}, at a relative humidity of 76 % RH and at injector positions of 30 (black points) and 80 cm (red points). The solid lines show the linear least-squares fit to the data, whose slopes are equal to $-0.25\gamma_{obs}wA_dt$ (see Eq. 3 in text). The HO_2 signal was averaged for 3 s at each point and the error bars represent one standard deviation.

so that the concentration of that component decreased rapidly over a few seconds:

$$HO_2 - S + X \rightarrow \text{products}. \quad \text{(R7)}$$

At higher HO_2 concentrations, X would be used up much faster than at low HO_2 concentrations, again resulting in a time dependence of the uptake coefficient along the flow tube. It is not possible from these experiments alone to determine which of the two proposed mechanisms is responsible for the observed HO_2 concentration dependence of the uptake coefficient, both of which also predict a time dependence. However, a model is currently being developed to further interpret the trends that have been observed.

3.2 The time dependence of the uptake coefficient

Measurements of the average uptake coefficients between $t = 0$ (when the HO_2 is injected) and six different reactions times (using the methodology used in Sect. 2.5) are shown in Fig. 8, for two different initial concentrations of HO_2. The results show that the uptake coefficient decreases with increasing time, suggesting (as introduced above in Sect. 3.1) that there is either a higher uptake coefficient for fresh aerosols followed by a lower uptake onto aerosols that have a partially saturated surface (Reactions R3–R6), or that a component in the aerosol which reacts with HO_2 is being used up over time (Reaction R7). A dependence of γ upon the HO_2 concentration can also be seen in Fig. 8, which also shows that the uptake coefficients do not approach zero at longer times, which would imply full equilibration (i.e. the rates of

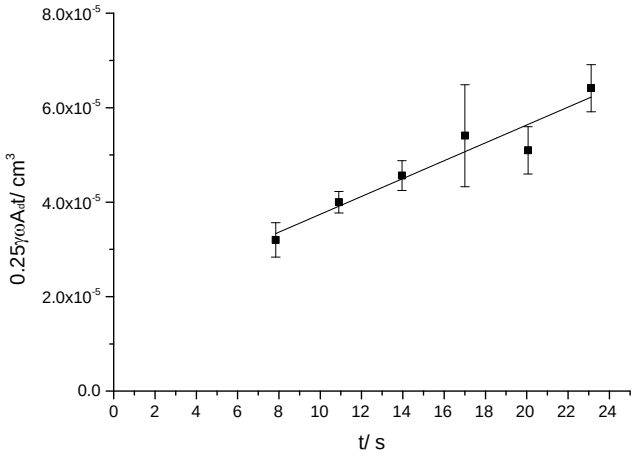

Figure 5. Plot of $0.25\gamma_{obs}wA_dt$ as a function of reaction time for uptake of HO_2 onto ATD aerosols. The linear least-squares fit to these point yields $0.25\gamma_{obs}wA_d$ as the gradient. The intercept of the fit at $t = 0$ ($(1.9 \pm 0.4) \times 10^{-5}$ cm^3) suggests a higher gradient and hence a higher uptake coefficient occurring in the first few seconds of contact between the HO_2 and ATD aerosols. The error bars represent two standard deviations in the individual exponential fits, examples of which are given in Fig. 4.

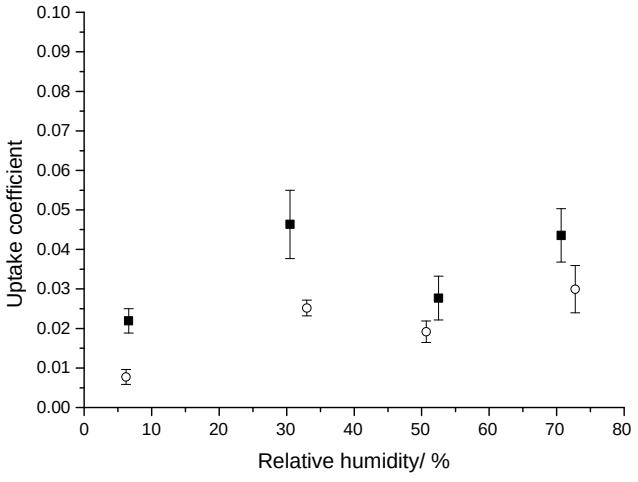

Figure 6. HO_2 uptake coefficients onto ATD aerosols measured at different relative humidities and at an initial HO_2 concentration of 1×10^9 (open symbols) and 3×10^8 molecule cm^{-3} (closed symbols). The error bars represent one standard deviation of the average of a number of repeated experiments.

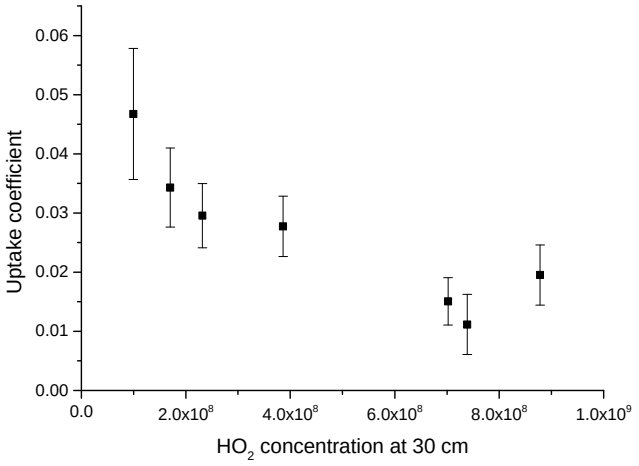

Figure 7. HO_2 uptake coefficients measured at different HO_2 concentrations, which were determined at an injector position of 30 cm when no dust aerosols were present in the aerosol flow tube. The error bars represent one standard deviation of a number of repeated experiments for a given HO_2 concentration.

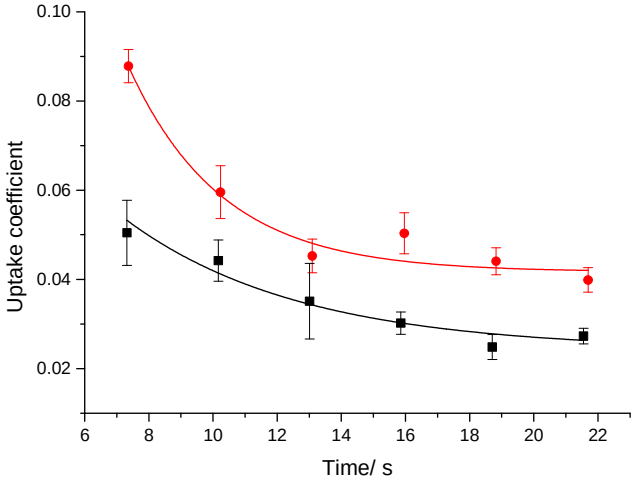

Figure 8. HO_2 uptake coefficients measured at a number of HO_2-aerosol contact times (corresponding to different injector positions). Experiments were performed at 10 % RH and at initial HO_2 concentrations of 1×10^9 (black squares) and 3×10^8 molecule cm^{-3} (red circles). The uptake coefficients correspond to the average value between $t = 0$ and the reaction time given. The error bars represent one standard deviation of the average of a number of repeated experiments. The solid lines are exponentially decaying functions $\gamma = 0.58\exp(-t/2.9) + 0.042$ and $\gamma = 0.11\exp(-t/5.4) + 0.024$ which are fitted to the data for 3×10^8 and 1×10^9 molecule cm^{-3}, respectively.

adsorption and desorption of HO_2 are equal). These results suggest that surface saturation (Reaction R3) is not the only process occurring and that there is also reaction at the dust surface which removes HO_2 irreversibly. The reaction of the HO_2 at the surface of the aerosol would become the rate-determining step once the aerosol surface was saturated. It would also be expected that the uptake coefficient would tend to zero if Reaction (R7) was solely responsible for the observation of the HO_2 concentration dependence and time dependence. However, fitting an exponentially decaying function to the data shown in Fig. 8 gave $\gamma = 0.042$ and 0.024 as the limiting values at long reaction times for $[HO_2] = 3 \times 10^8$ and 1×10^9 molecule cm^{-3}, respectively. These values are within

the error bars of 0.031 ± 0.008 and 0.018 ± 0.006 measured as the average from Fig. 6.

3.3 Comparison of γ_{HO_2} with literature values

Bedjanian et al. (2013) is the only published study to our knowledge reporting a HO_2 uptake coefficient onto solid ATD surfaces, which reported initial uptake coefficients (γ_0) onto fresh ATD surfaces and for HO_2 concentrations in the range of $0.35–3.30 \times 10^{12}$ molecule cm^{-3}. In the work reported here aerosols were used instead of a coated surface and HO_2 concentrations were approximately four orders of magnitude lower. Bedjanian et al. (2013) observed an order of magnitude decrease in the uptake coefficient (from $\gamma_0 \sim 0.07$ to $\gamma_0 \sim 0.007$ at 275 K) when increasing the relative humidity between 0.02 and 94 %, which was attributed to water molecules binding to the dust surface and blocking the active sites for incoming HO_2 radicals. A similar humidity dependence has also been observed by Remorov et al. (2002) for HO_2 uptake onto solid sodium chloride surfaces and by Loukhovitskaya et al. (2009) for HO_2 uptake onto $MgCl_2 \cdot 6\,H_2O$ surfaces. However, Loukhovitskaya et al. (2009) did not see a humidity dependence for NaCl or NaBr surfaces. Contrastingly, Taketani and Kanaya (2010) and Taketani et al. (2008, 2013) reported a small increase in uptake coefficient with humidity for a variety of different solid aerosols which was attributed to HO_2–H_2O complexes being formed on the surface of the aerosols. In the work reported here, a small increase in uptake was also observed with increasing humidity. However, this apparent dependence was attributed to a HO_2 concentration effect, with higher humidities leading to lower HO_2 concentrations due to the higher wall losses and higher measured uptake coefficients.

Bedjanian et al. (2013) did not observe a HO_2 concentration dependence. However, this may be due to the fact that γ_0, the initial uptake onto a fresh surface, was measured rather than uptake onto dust which had already been partially saturated by HO_2. However, Bedjanian et al. (2013) did observe a time dependence over ~ 80 min that was attributed to deactivation of the dust surface. The deactivation of a solid surface has previously been suggested as being due to the by-products from reactions used to form HO_2 (e.g. HF as used by Bedjanian et al.) (Loukhovitskaya et al., 2009). However, as reported in this paper, HO_2 was formed from the photolysis of water vapour in the presence of trace levels of O_2 so, other than OH, which is completely removed within the injector, to our knowledge there should be no other products from our method of HO_2 generation that could deactivate the surface. An uptake coefficient dependence upon time and radical concentration has also been observed for other species onto solid surfaces and has been attributed to surface saturation or to a component of an aerosol being used up over time (Ammann and Pöschl, 2007; Shiraiwa et al., 2012; Slade and Knopf, 2013). Crowley et al. (2010) have also discussed the drawbacks of using bulk samples and the geometric area of sample holders to investigate heterogeneous reactions.

In this laboratory, George et al. (2013) previously measured uptake coefficients onto aqueous and dry salt aerosols using a very similar setup described in this paper and with an initial HO_2 concentration of 1×10^9 molecule cm^{-3}. For dry salts, the uptake coefficient was below the limit of detection (<0.004) and for aqueous salts the uptake coefficient was measured as being between 0.003 and 0.016 depending on humidity and the type of salt. Therefore, the value of 0.018 ± 0.006 measured for $[HO_2] = 1 \times 10^9$ molecule cm^{-3} for ATD aerosols shows that the HO_2 uptake coefficient of ATD is larger than for salt aerosols. The larger values for dust aerosols compared to solid dry salts may be due to the non-sphericity of the aerosols, leading to much larger surface areas for ATD (the Brunauer–Emmett–Teller (BET) surface area for ATD was determined by Bedjanian et al. (2013) as 85 ± 10 m^2 g^{-1}), or may due to the chemical composition of the aerosols, for example the presence of transition metal ions.

4 Atmospheric implications

A box model which contains a near explicit chemical scheme for the oxidative degradation of C1–C5 hydrocarbons, taken from the master chemical mechanism (MCM) version 3.1 (Saunders et al., 2003) has been used to assess the atmospheric impact of heterogeneous loss of HO_2 concentrations to dust particles. The model was constrained with gas-phase data taken during the Reactive Halogens in the Marine Boundary Layer (RHaMBLe) project (Lee et al., 2010) that took place in 2007 at the Cape Verde Atmospheric Observatory (CVAO; Carpenter et al., 2010), which is situated on the island of Sao Vicente in the tropical Atlantic Ocean (23.96° S, 46.39° W). The model has been used previously to calculate OH and HO_2 concentrations for comparison with those measured at CVAO (Whalley et al., 2010). Hourly measurements of VOCs such as ethane, acetaldehyde, methanol, acetone and formaldehyde, NO_x, O_3, CO, CH_4, $j(O^1D)$ and meteorological parameters were used to constrain the model. A halogen chemical scheme was also included in the mechanism (Whalley et al., 2010) and the model was constrained to average diurnal cycles of IO and BrO radicals which were measured by long-path differential optical absorption spectroscopy (DOAS) at the observatory in May 2007 (Read et al., 2008). A constant HCHO concentration of 328 pptv (parts per trillion by volume), based on average [HCHO] measured by LP-DOAS (Whalley et al., 2010), and a constant H_2 concentration of 500 ppb (parts per billion), typical of MBL concentrations, were used as constraints.

A simple scheme, based on a first-order loss of HO_2 to aerosol surfaces (Ravishankara, 1997) was considered in the model to determine the impact of dust particles:

$$k'_{\text{loss}} = \frac{wA\gamma}{4}, \quad (10)$$

where w is the mean molecular speed of HO_2 molecules (cm s^{-1}), defined in Eq. (4), k_{loss} is the heterogeneous loss rate, A is the aerosol surface area per unit volume and γ is the uptake coefficient (determined from the experiments reported in this work). The model was run to steady state ($\sim$ 4 days) using the FACSIMILE integrator (Sweetenham and Curtis, 1987) at which point the diurnal variation of unmeasured model intermediates remained constant.

Cape Verde is predominantly affected by marine aerosols and is also seasonally affected by Saharan dust particles with more dust events observed during the winter (Müller et al., 2010). Although HO_2 uptake experiments have been performed in this work using ATD rather than Saharan dust, previous experiments for NO_2 and NO_3 uptake onto both types of surface have produced almost identical uptake coefficients, whilst for N_2O_5 and HNO_3 the measured uptake was approximately a factor of 1.5–2 lower for ATD (Crowley et al., 2010; Tang et al., 2014).

When running the model it was assumed that no products, such as H_2O_2, generated from the uptake of HO_2 by dust surfaces, were released to the gas phase, and the temperature was inputted into the model and varied depending on the time of day with an average temperature of 296 K. The rate of uptake of other species onto dust aerosol surfaces was set to zero. The model calculated a maximum HO_2 concentration at solar noon of 1.9×10^8 molecule cm^{-3} ($\sim$ 7.5 pptv) with no aerosols present. The HO_2 uptake coefficient was then fixed to $\gamma = 0.031 \pm 0.008$, the value obtained in this work for ATD aerosols for the lower HO_2 concentrations used in the experiments. The value of $\gamma = 0.031 \pm 0.008$ was on the higher side of the observed range of HO_2 uptake coefficients measured in this work. Assuming an average aerosol diameter of 1 µm and a density of 2.7 g cm^{-3}, a typical range of dust aerosol concentrations of 10–200 $\mu\text{g m}^{-3}$ observed in Cape Verde (throughout the SAMUM-2 field campaign) (Schladitz et al., 2011) corresponds to geometric surface areas of 2.2×10^{-7}–4.4×10^{-6} $\text{cm}^2\,\text{cm}^{-3}$, respectively. For this range of surface areas, the box model constrained by Cape Verde conditions calculated a decrease in the maximum HO_2 concentrations from the no aerosol value of between 0.3 and 6.5 %. The impact on the maximum noon HO_2 concentration due to varying the total dust surface area and $\gamma = 0.031$ is shown in Fig. 9. Given the variation of γ with $[HO_2]$ as shown in Fig. 7, the percentage reduction in HO_2 due to heterogeneous uptake onto dust may be greater than shown in Fig. 9 in the morning and evening when $[HO_2]$ is lower. It should be noted that diffusive limitations due to the larger aerosol diameters were disregarded in these calculations.

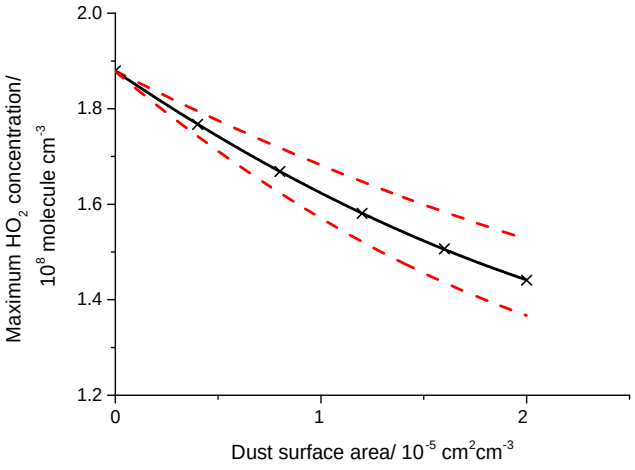

Figure 9. The decrease of the solar noon maximum HO_2 concentration (crosses with solid black line) with dust surface area calculated by a box model utilising the master chemical mechanism and constrained to conditions at the Cape Verde Atmospheric Observatory. An HO_2 uptake coefficient of 0.031 was used in these calculations, and the dashed red lines represent the HO_2 concentrations calculated with the $\pm$0.008 error in the uptake coefficient.

During the RHaMBLe campaign, which started in May 2007, high dust concentrations (40–69 $\mu\text{g m}^{-3}$) were only measured for the first 3 days of the campaign, although during a dust event in the previous week a dust concentration of 332 $\mu\text{g m}^{-3}$ had been measured (Müller et al., 2010). During the remainder of the RHaMBLe campaign the dust concentrations were typically less than 10 $\mu\text{g m}^{-3}$ (Müller et al., 2010). Whalley et al. (2010) reported that in order to obtain good agreement between HO_2 model predictions and observations during RHaMBLe, HO_2 aerosol uptake and deposition to the ocean had to account for 23 % of the total rate of HO_2 loss at noon. However, with dust concentrations of less than 10 $\mu\text{g m}^{-3}$ during the model–measurement comparison period, the HO_2 concentrations would be affected by less than 0.3 %. The dust loading though at Cape Verde is highly variable, and the loading of 332 $\mu\text{g m}^{-3}$ mentioned above would reduce HO_2 by over 10 % from uptake onto dust alone.

Soot and silicate particles have also been found in the fine particle modes in Cape Verde (Schladitz et al., 2011). The impact on HO_2 concentrations due to uptake onto these particles is unknown due to a lack of laboratory data. Sea-salt aerosols could also contribute significantly to the difference between the models and observations, especially if they contain small amounts of transition metal ions (Fitzsimmons et al., 2013), such as copper, which has been shown in laboratory studies to increase the HO_2 uptake coefficient significantly (George et al., 2013; Mozurkewich et al., 1987; Taketani et al., 2008; Thornton and Abbatt, 2005). Uptake coefficients of N_2O_5 to illite aerosols ($\gamma = 0.04$–0.09, dependent upon RH), which is one of the most abundant clay minerals in

dust, were measured to be considerably larger than for uptake to ATD ($\gamma \sim 0.006$, weak if any dependence upon RH) (Tang et al., 2014). Hence future studies measuring the uptake of HO_2 onto illite and other components of dust aerosols, as well on Saharan or Asian dust samples, would be highly beneficial.

5 Conclusions

HO_2 uptake coefficients onto dust aerosols were measured for the first time using a flow tube reactor coupled with a sensitive HO_2 FAGE detection system. The HO_2 uptake coefficient on Arizona test dust aerosol was measured as $\gamma = 0.031 \pm 0.008$ and $\gamma = 0.018 \pm 0.006$ for initial HO_2 concentrations of 3×10^8 and 1×10^9 molecule cm^{-3}, respectively, with very little dependence upon relative humidity observed over a wide range (6–76 %). Both a HO_2 concentration dependence and a time dependence on the uptake coefficient was observed, suggesting that the active sites on the dust surface were becoming blocked by either HO_2 or a reaction product, or that a component of the dust that removed HO_2 by reaction was being used up over time. However, for both the lower and higher HO_2 concentrations the time dependence of the uptake coefficient did not approach zero at long times, indicating that there was a slow reaction on the surface removing HO_2.

The atmospheric impact of the uptake onto dust aerosols on HO_2 concentrations was investigated for the conditions encountered at the Cape Verde Atmospheric Observatory in the tropical Atlantic Ocean. Over the range of dust aerosol concentrations encountered at Cape Verde there was a significant effect on HO_2 concentrations, lowering them by more than 10 % for the higher loadings of aerosols that are common during winter. However, dust aerosols alone probably cannot account for the entire difference between measured and modelled HO_2 concentrations that was observed during the RHaMBLe field campaign in 2007. In order to be able to reduce the difference between measured and modelled concentrations from uptake onto aerosols, more information is needed about transition metal ion concentrations in marine aerosols as well as further measurements of HO_2 uptake coefficients onto other type or aerosols; for example, soot, silicate and other mineral particles. The modelling studies also showed that in regions with much higher dust concentrations (e.g. the sub-Saharan Africa), the impact on HO_2 concentrations may be even more important. Indeed, during a pre-monsoon dust storm in northern India, a study using the Weather Research and Forecasting model coupled with Chemistry (WRF-Chem) showed that uptake of HO_2 via heterogeneous reactions on dust surfaces led to a maximum reduction of about 40 % over the Thar Desert study region (Kumar et al., 2014), using the value of γ determined by Bedjanian et al. (2013).

Acknowledgements. This work was supported by the National Environment Research Council under grant NE/F020651/1. P. S. J. Matthews is grateful to NERC for the award of a studentship. L. K. Whalley and D. E. Heard are also grateful to the NERC funded National Centre for Atmospheric Science for ongoing support. We are grateful to the Centre for Atmospheric Science in the School of Earth Atmospheric and Environmental Sciences at the University of Manchester for the loan of the aerodynamic particle sizer used in this work.

Edited by: F. Keutsch

References

Ammann, M. and Pöschl, U.: Kinetic model framework for aerosol and cloud surface chemistry and gas-particle interactions – Part 2: Exemplary practical applications and numerical simulations, Atmos. Chem. Phys., 7, 6025–6045, doi:10.5194/acp-7-6025-2007, 2007.

Bedjanian, Y., Romanias, M. N., and El Zein, A.: Uptake of HO_2 radicals on Arizona Test Dust, Atmos. Chem. Phys., 13, 6461–6471, doi:10.5194/acp-13-6461-2013, 2013.

Bloss, W. J., Lee, J. D., Johnson, G. P., Sommariva, R., Heard, D. E., Saiz-Lopez, A., Plane, J. M. C., McFiggans, G., Coe, H., Flynn, M., Williams, P., Rickard, A. R., and Fleming, Z. L.: Impact of halogen monoxide chemistry upon boundary layer OH and HO_2 concentrations at a coastal site, Geophys. Res. Lett., 32, L06814, doi:10.1029/2004GL022084, 2005.

Brown, R. L.: Tubular Flow Reactors With 1st-Order Kinetics, J. Res. Nat. Bur. Stand., 83, 1–8, 1978.

Brune, W. H., Tan, D., Faloona, I. F., Jaegle, L., Jacob, D. J., Heikes, B. G., Snow, J., Kondo, Y., Shetter, R., Sachse, G. W., Anderson, B., Gregory, G. L., Vay, S., Singh, H. B., Davis, D. D., Crawford, J. H., and Blake, D. R.: OH and HO_2 chemistry in the North Atlantic free troposphere, Geophys. Res. Lett., 26, 3077–3080, 1999.

Cantrell, C. A., Shetter, R. E., Gilpin, T. M., and Calvert, J. G.: Peroxy radicals measured during Mauna Loa observatory photochemistry experiment 2: The data and first analysis, J. Geophys. Res.-Atmos., 101, 14643–14652, 1996.

Carpenter, L. J., Fleming, Z. L., Read, K. A., Lee, J. D., Moller, S. J., Hopkins, J. R., Purvis, R. M., Lewis, A. C., Müller, K., Heinold, B., Herrmann, H., Fomba, K. W., Pinxteren, D., Müller, C., Tegen, I., Wiedensohler, A., Müller, T., Niedermeier, N., Achterberg, E. P., Patey, M. D., Kozlova, E. A., Heimann, M., Heard, D. E., Plane, J. M. C., Mahajan, A., Oetjen, H., Ingham, T., Stone, D., Whalley, L. K., Evans, M. J., Pilling, M. J., Leigh, R. J., Monks, P. S., Karunaharan, A., Vaughan, S., Arnold, S. R., Tschritter, J., Pöhler, D., Frieß, U., Holla, R., Mendes, L. M., Lopez, H., Faria, B., Manning, A. J., and Wallace, D. W. R.: Seasonal characteristics of tropical marine boundary layer air measured at the Cape Verde Atmospheric Observatory, J. Atmos. Chem., 67, 87–140, 2010.

Carslaw, N., Creasey, D. J., Heard, D. E., Lewis, A. C., McQuaid, J. B., Pilling, M. J., Monks, P. S., Bandy, B. J., and Penkett, S. A.: Modeling OH, HO_2, and RO_2 radicals in the marine boundary layer – 1. Model construction and comparison with field measurements, J. Geophys. Res.-Atmos., 104, 30241–30255, 1999.

Carslaw, N., Creasey, D. J., Heard, D. E., Jacobs, P. J., Lee, J. D., Lewis, A. C., McQuaid, J. B., Pilling, M. J., Bauguitte, S., Penkett, S. A., Monks, P. S., and Salisbury, G.: Eastern Atlantic Spring Experiment 1997 (EASE97) – 2. Comparisons of model concentrations of OH, HO_2, and RO_2 with measurements, J. Geophys. Res.-Atmos., 107, ACH 5-1–ACH 5-16, doi:10.1029/2001JD001568, 2002.

Crowley, J. N., Ammann, M., Cox, R. A., Hynes, R. G., Jenkin, M. E., Mellouki, A., Rossi, M. J., Troe, J., and Wallington, T. J.: Evaluated kinetic and photochemical data for atmospheric chemistry: Volume V – heterogeneous reactions on solid substrates, Atmos. Chem. Phys., 10, 9059–9223, doi:10.5194/acp-10-9059-2010, 2010.

Dentener, F. J., Carmichael, G. R., Zhang, Y., Lelieveld, J., and Crutzen, P. J.: Role of mineral aerosol as a reactive surface in the global troposphere, J. Geophys. Res.-Atmos., 101, 22869–22889, 1996.

Fitzsimmons, J. N., Zhang, R., and Boyle, E. A.: Dissolved iron in the tropical North Atlantic Ocean, Mar. Chem., 154, 87–99, 2013.

George, I. J., Matthews, P. S. J., Whalley, L. K., Brooks, B., Goddard, A., Baeza-Romero, M. T., and Heard, D. E.: Measurements of uptake coefficients for heterogeneous loss of HO_2 onto submicron inorganic salt aerosols, Phys. Chem. Chem. Phys., 15, 12829–12845, 2013.

Haggerstone, A. L., Carpenter, L. J., Carslaw, N., and McFiggans, G.: Improved model predictions of HO_2 with gas to particle mass transfer rates calculated using aerosol number size distributions, J. Geophys. Res.-Atmos., 110, D04304, doi:10.1029/2004JD005282, 2005.

Hinds, W. C.: Aerosol technology : properties, behavior, and measurement of airborne particles/William C. Hinds, Wiley, New York, Chichester, 1982.

Jaegle, L., Jacob, D. J., Brune, W. H., Faloona, I., Tan, D., Heikes, B. G., Kondo, Y., Sachse, G. W., Anderson, B., Gregory, G. L., Singh, H. B., Pueschel, R., Ferry, G., Blake, D. R., and Shetter, R. E.: Photochemistry of HO_x in the upper troposphere at northern midlatitudes, J. Geophys. Res.-Atmos., 105, 3877-3892, 2000.

Kanaya, Y., Sadanaga, Y., Matsumoto, J., Sharma, U. K., Hirokawa, J., Kajii, Y., and Akimoto, H.: Daytime HO_2 concentrations at Oki Island, Japan, in summer 1998: Comparison between measurement and theory, J. Geophys. Res.-Atmos., 105, 24205–24222, doi:10.1029/2001GL014061, 2000.

Kanaya, Y., Yokouchi, Y., Matsumoto, J., Nakamura, K., Kato, S., Tanimoto, H., Furutani, H., Toyota, K., and Akimoto, H.: Implications of iodine chemistry for daytime HO_2 levels at Rishiri Island, Geophys. Res. Lett., 29, 1212, doi:10.1029/2006JD007987, 2002.

Kanaya, Y., Cao, R., Kato, S., Miyakawa, Y., Kajii, Y., Tanimoto, H., Yokouchi, Y., Mochida, M., Kawamura, K., and Akimoto, H.: Chemistry of OH and HO_2 radicals observed at Rishiri Island, Japan, in September 2003: Missing daytime sink of $HO_2$and positive nighttime correlations with monoterpenes, J. Geophys. Res.-Atmos., 112, D11308, doi:10.1029/2006JD007987, 2007.

Karagulian, F., Santschi, C., and Rossi, M. J.: The heterogeneous chemical kinetics of N_2O_5 on $CaCO_3$ and other atmospheric mineral dust surrogates, Atmos. Chem. Phys., 6, 1373–1388, doi:10.5194/acp-6-1373-2006, 2006.

Kumar, R., Barth, M. C., Madronich, S., Naja, M., Carmichael, G. R., Pfister, G. G., Knote, C., Brasseur, G. P., Ojha, N., and Sarangi, T.: Effects of dust aerosols on tropospheric chemistry during a typical pre-monsoon season dust storm in northern India, Atmos. Chem. Phys. Discuss., 14, 1113–1158, doi:10.5194/acpd-14-1113-2014, 2014.

Lee, J. D., McFiggans, G., Allan, J. D., Baker, A. R., Ball, S. M., Benton, A. K., Carpenter, L. J., Commane, R., Finley, B. D., Evans, M., Fuentes, E., Furneaux, K., Goddard, A., Good, N., Hamilton, J. F., Heard, D. E., Herrmann, H., Hollingsworth, A., Hopkins, J. R., Ingham, T., Irwin, M., Jones, C. E., Jones, R. L., Keene, W. C., Lawler, M. J., Lehmann, S., Lewis, A. C., Long, M. S., Mahajan, A., Methven, J., Moller, S. J., Müller, K., Müller, T., Niedermeier, N., O'Doherty, S., Oetjen, H., Plane, J. M. C., Pszenny, A. A. P., Read, K. A., Saiz-Lopez, A., Saltzman, E. S., Sander, R., von Glasow, R., Whalley, L., Wiedensohler, A., and Young, D.: Reactive Halogens in the Marine Boundary Layer (RHaMBLe): the tropical North Atlantic experiments, Atmos. Chem. Phys., 10, 1031–1055, doi:10.5194/acp-10-1031-2010, 2010.

Loukhovitskaya, E., Bedjanian, Y., Morozov, I., and Le Bras, G.: Laboratory study of the interaction of HO_2 radicals with the NaCl, NaBr, $MgCl_2 \cdot 6\,H_2O$ and sea salt surfaces, Phys. Chem. Chem. Phys., 11, 7896–7905, 2009.

Mao, J., Jacob, D. J., Evans, M. J., Olson, J. R., Ren, X., Brune, W. H., Clair, J. M. St., Crounse, J. D., Spencer, K. M., Beaver, M. R., Wennberg, P. O., Cubison, M. J., Jimenez, J. L., Fried, A., Weibring, P., Walega, J. G., Hall, S. R., Weinheimer, A. J., Cohen, R. C., Chen, G., Crawford, J. H., McNaughton, C., Clarke, A. D., Jaeglé, L., Fisher, J. A., Yantosca, R. M., Le Sager, P., and Carouge, C.: Chemistry of hydrogen oxide radicals (HO_x) in the Arctic troposphere in spring, Atmos. Chem. Phys., 10, 5823–5838, doi:10.5194/acp-10-5823-2010, 2010.

Mozurkewich, M., McMurry, P. H., Gupta, A., and Calvert, J. G.: Mass Accommodation Coefficient For HO_2 Radicals On Aqueous Particles, J. Geophys. Res.-Atmos., 92, 4163–4170, 1987.

Müller, K., Lehmann, S., van Pinxteren, D., Gnauk, T., Niedermeier, N., Wiedensohler, A., and Herrmann, H.: Particle characterization at the Cape Verde atmospheric observatory during the 2007 RHaMBLe intensive, Atmos. Chem. Phys., 10, 2709–2721, doi:10.5194/acp-10-2709-2010, 2010.

Ravishankara, A. R.: Heterogeneous and multiphase chemistry in the troposphere, Science, 276, 1058–1065, 1997.

Remorov, R. G., Gershenzon, Y. M., Molina, L. T., and Molina, M. J.: Kinetics and mechanism of HO_2 uptake on solid NaCl, J. Phys. Chem. A, 106, 4558–4565, 2002.

Saunders, S. M., Jenkin, M. E., Derwent, R. G., and Pilling, M. J.: Protocol for the development of the Master Chemical Mechanism, MCM v3 (Part A): tropospheric degradation of non-aromatic volatile organic compounds, Atmos. Chem. Phys., 3, 161–180, doi:10.5194/acp-3-161-2003, 2003.

Schladitz, A., Mueller, T., Nowak, A., Kandler, K., Lieke, K., Massling, A., and Wiedensohler, A.: In situ aerosol characterization at Cape Verde Part 1: Particle number size distributions, hygroscopic growth and state of mixing of the marine and Saharan dust aerosol, Tellus B, 63, 531–548, 2011.

Seinfeld, J. H. and Pandis, S. N.: Atmospheric chemistry and physics: from air pollution to climate change, Wiley, 2006.

Shiraiwa, M., Pöschl, U., and Knopf, D. A.: Multiphase Chemical Kinetics of NO3 Radicals Reacting with Organic Aerosol Components from Biomass Burning, Environ. Sci. Technol., 46, 6630–6636, 2012.

Slade, J. H. and Knopf, D. A.: Heterogeneous OH oxidation of biomass burning organic aerosol surrogate compounds: assessment of volatilisation products and the role of OH concentration on the reactive uptake kinetics, Phys. Chem. Chem. Phys., 15, 5898–5915, 2013.

Smith, S. C., Lee, J. D., Bloss, W. J., Johnson, G. P., Ingham, T., and Heard, D. E.: Concentrations of OH and HO_2 radicals during NAMBLEX: measurements and steady state analysis, Atmos. Chem. Phys., 6, 1435–1453, doi:10.5194/acp-6-1435-2006, 2006.

Sommariva, R., Haggerstone, A.-L., Carpenter, L. J., Carslaw, N., Creasey, D. J., Heard, D. E., Lee, J. D., Lewis, A. C., Pilling, M. J., and Zádor, J.: OH and HO_2 chemistry in clean marine air during SOAPEX-2, Atmos. Chem. Phys., 4, 839–856, doi:10.5194/acp-4-839-2004, 2004.

Sommariva, R., Bloss, W. J., Brough, N., Carslaw, N., Flynn, M., Haggerstone, A.-L., Heard, D. E., Hopkins, J. R., Lee, J. D., Lewis, A. C., McFiggans, G., Monks, P. S., Penkett, S. A., Pilling, M. J., Plane, J. M. C., Read, K. A., Saiz-Lopez, A., Rickard, A. R., and Williams, P. I.: OH and HO_2 chemistry during NAMBLEX: roles of oxygenates, halogen oxides and heterogeneous uptake, Atmos. Chem. Phys., 6, 1135–1153, doi:10.5194/acp-6-1135-2006, 2006.

Stevens, P. S., Mather, J. H., and Brune, W. H.: Measurement of tropospheric OH and HO_2 by Laser Induced Fluorescence at low pressure, J. Geophys. Res.-Atmos., 99, 3543–3557, 1994.

Stone, D., Whalley, L. K., and Heard, D. E.: Tropospheric OH and HO_2 radicals: field measurements and model comparisons, Chem. Soc. Rev., 41, 6348–6404, 2012.

Sweetenham, W. P. and Curtis, A. R.: FACSIMILE/CHEKMAT User's Manual, Harwell Laboratory, Oxfordshire, Great Britain, 1987.

Taketani, F. and Kanaya, Y.: Kinetics of HO_2 Uptake in Levoglucosan and Polystyrene Latex Particles, J. Phys. Chem. Lett., 1, 1701–1704, 2010.

Taketani, F., Kanaya, Y., and Akimoto, H.: Kinetics of heterogeneous reactions of HO_2 radical at ambient concentration levels with $(NH_4)_2SO_4$ and NaCl aerosol particles, J. Phys. Chem. A, 112, 2370–2377, 2008.

Taketani, F., Kanaya, Y., and Akimoto, H.: Kinetic Studies of Heterogeneous Reaction of HO_2 Radical by Dicarboxylic Acid Particles, International J. Chem. Kinet., 45, 560–565, 2013.

Tang, M. J., Thieser, J., Schuster, G., and Crowley, J. N.: Kinetics and mechanism of the heterogeneous reaction of N_2O_5 with mineral dust particles, Phys. Chem. Chem. Phys., 14, 8551–8561, 2012.

Tang, M. J., Schuster, G., and Crowley, J. N.: Heterogeneous reaction of N_2O_5 with illite and Arizona test dust particles, Atmos. Chem. Phys., 14, 245–254, doi:10.5194/acp-14-245-2014, 2014.

Textor, C., Schulz, M., Guibert, S., Kinne, S., Balkanski, Y., Bauer, S., Berntsen, T., Berglen, T., Boucher, O., Chin, M., Dentener, F., Diehl, T., Easter, R., Feichter, H., Fillmore, D., Ghan, S., Ginoux, P., Gong, S., Grini, A., Hendricks, J., Horowitz, L., Huang, P., Isaksen, I., Iversen, I., Kloster, S., Koch, D., Kirkevåg, A., Kristjansson, J. E., Krol, M., Lauer, A., Lamarque, J. F., Liu, X., Montanaro, V., Myhre, G., Penner, J., Pitari, G., Reddy, S., Seland, Ø., Stier, P., Takemura, T., and Tie, X.: Analysis and quantification of the diversities of aerosol life cycles within AeroCom, Atmos. Chem. Phys., 6, 1777–1813, doi:10.5194/acp-6-1777-2006, 2006.

Thornton, J. and Abbatt, J. P. D.: Measurements of HO_2 uptake to aqueous aerosol: Mass accommodation coefficients and net reactive loss, J. Geophys. Res.-Atmos., 110, D08309, doi:10.1029/2004JD005402, 2005.

Vaughan, S., Ingham, T., Whalley, L. K., Stone, D., Evans, M. J., Read, K. A., Lee, J. D., Moller, S. J., Carpenter, L. J., Lewis, A. C., Fleming, Z. L., and Heard, D. E.: Seasonal observations of OH and HO_2 in the remote tropical marine boundary layer, Atmos. Chem. Phys., 12, 2149–2172, doi:10.5194/acp-12-2149-2012, 2012.

Wagner, C., Hanisch, F., Holmes, N., de Coninck, H., Schuster, G., and Crowley, J. N.: The interaction of N_2O_5 with mineral dust: aerosol flow tube and Knudsen reactor studies, Atmos. Chem. Phys., 8, 91–109, doi:10.5194/acp-8-91-2008, 2008.

Whalley, L. K., Furneaux, K. L., Goddard, A., Lee, J. D., Mahajan, A., Oetjen, H., Read, K. A., Kaaden, N., Carpenter, L. J., Lewis, A. C., Plane, J. M. C., Saltzman, E. S., Wiedensohler, A., and Heard, D. E.: The chemistry of OH and HO_2 radicals in the boundary layer over the tropical Atlantic Ocean, Atmos. Chem. Phys., 10, 1555–1576, doi:10.5194/acp-10-1555-2010, 2010.